Applied Physics Letters

Terahertz amplification in RTD-gated HEMTs with a grating-gate wave coupling topology

Cite as: Appl. Phys. Lett. **109**, 063111 (2016); https://doi.org/10.1063/1.4961053
Submitted: 23 April 2016 . Accepted: 03 August 2016 . Published Online: 11 August 2016

Hugo O. Condori Quispe, Jimy J. Encomendero-Risco, Huili Grace Xing, and Berardi Sensale-Rodriguez

View Online

Export Citation

CrossMark

ARTICLES YOU MAY BE INTERESTED IN

Resonant tunneling assisted propagation and amplification of plasmons in high electron mobility transistors
Journal of Applied Physics **119**, 013102 (2016); https://doi.org/10.1063/1.4939076

Terahertz spectroscopy of an electron-hole bilayer system in AlN/GaN/AlN quantum wells
Applied Physics Letters **111**, 073102 (2017); https://doi.org/10.1063/1.4996925

Electrically driven terahertz radiation of 2DEG plasmons in AlGaN/GaN structures at 110 K temperature
Applied Physics Letters **110**, 202101 (2017); https://doi.org/10.1063/1.4983286

Lock-in Amplifiers
Find out more today

Zurich Instruments

AIP Publishing

© 2016 Author(s).

Terahertz amplification in RTD-gated HEMTs with a grating-gate wave coupling topology

Hugo O. Condori Quispe,[1] Jimy J. Encomendero-Risco,[2,3] Huili Grace Xing,[2,3] and Berardi Sensale-Rodriguez[1]
[1]*The University of Utah, Salt Lake City, Utah 84112, USA*
[2]*University of Notre Dame, Notre Dame, Indiana 46556, USA*
[3]*Cornell University, Ithaca, New York 14853, USA*

(Received 23 April 2016; accepted 3 August 2016; published online 11 August 2016)

We theoretically analyze the operation of a terahertz amplifier consisting of a resonant-tunneling-diode gated high-electron-mobility transistor (RTD-gated HEMT) in a grating-gate topology. In these devices, the key element enabling substantial power gain is the efficient coupling of terahertz waves into and out of plasmons in the RTD-gated HEMT channel, i.e., the gain medium, via the grating-gate itself, part of the active device, rather than by an external antenna structure as discussed in previous works, therefore potentially enabling terahertz amplification with associated power gains >40 dB. *Published by AIP Publishing.* [http://dx.doi.org/10.1063/1.4961053]

Over the past decades, the terahertz region of the spectrum has become the subject of much attention due to its wide range of applications including astronomy, imaging, spectroscopy, communications, etc.[1–3] Although important progress has been recently achieved, there is still a significant need for devices efficiently operating at these frequencies, for instance, enabling power amplification. In this context, resonant-tunneling-diode-gated high-electron-mobility transistors (RTD-gated HEMTs) have been recently proposed as terahertz amplifiers.[4]

In this letter, we present our theoretical evaluation of power amplification in RTD-gated HEMTs with a grating gate topology to couple in and out an incoming normally incident terahertz beam. In these devices, gain originates from the interplay between the gate-to-channel negative differential conductance and electron-plasma-waves in the HEMT channel, acting collectively as a gain medium.[5–7] This work differs from our previous work,[4] in that coupling of the terahertz radiation into electron-plasma-waves is integrated via the grating-gate itself, which can be considered as an intrinsic part of the active device, instead of via an external antenna structure built around the active device.[4] As discussed by Popov in Ref. 8, in the context of HEMT terahertz detectors, a sub-wavelength grating-gate placed close to the HEMT channel acts as an aerial matched antenna allowing to efficiently couple the incoming terahertz waves to electron-plasma-waves along the channel thus leading to an enhanced HEMT terahertz detector responsivity. *Via numerical simulations for RTD-gated HEMTs under this grating-gate configuration, we show that (i) the electrical conductivities of the gated and ungated regions of the device, (ii) the negative differential conductance level achievable from the RTD, and (iii) the filling-factor, are important parameters affecting the attainable power gain levels as well as the stability in this device.*

According to Dyakonov and Shur theory,[9,10] the two-dimensional electron gas (2DEG) in the HEMT channel allows for collective motion of electrons, i.e., electron-plasma-waves, as demonstrated in, e.g., Refs. 11–14. In this context, the gate length geometrically defines a resonant cavity where excitation of electron-plasma-waves is possible. In these structures, the velocity of the plasma-waves can be one order of magnitude larger than the electron drift velocity thus allowing these plasma-wave resonances to fall in the terahertz range.

Electron-plasma-wave resonances in grating-gate structures have been first observed by Allen *et al.*[15] In this case, a silicon inversion layer at cryogenic temperature was employed as the 2DEG where electron-plasma-waves were excited. Experimental observation of electron-plasma-wave resonances was later shown in various materials, e.g., in GaN by Muravjov *et al.*,[13] in graphene by Ju *et al.*,[16] etc. The transmission spectra in these grating-gate structures show a strong coupling between the electron-plasma-waves in the 2DEG and an incoming normally incident terahertz beam. The set of plasma-wave modes supported in these grating-gate HEMT structures is given by[2,13,15,17–19]

$$\omega_p^2 = (n_s e^2/m^*).k/\varepsilon_0(\varepsilon_s + \varepsilon_b \coth(kd)), \quad (1)$$

where e is the electron charge, ε_0 is the vacuum permittivity, ε_s and ε_b are the relative permittivity of the layers below and above the 2DEG, respectively, d is the barrier thickness, m^* is the electron effective mass, n_s is the electron concentration, k is the magnitude of the plasma wave vector ($k = 2\pi/L$), and L is the unit cell period.

The discussion in this work will be based on numerical simulations of grating-gate RTD-gated HEMTs. In the first stage, so to show the validity of numerical simulations in order to represent electron-plasma-wave phenomena, we proceeded to simulate the grating-gate HEMT structure discussed in Ref. 13 employing a layer-by-layer model in Ansys High Frequency Structural Simulator (HFSS). For this purpose, each layer in the epitaxial structure is modelled by means of a set of constitutive parameters: ε, σ, and μ. The terahertz excitation is defined as a normally incident plane-wave (with respect to the sample), i.e., a plane wave-propagating along the z-axis, and with polarization perpendicular to the gate fingers (i.e., along x-direction). Due to the symmetry of the device structure, periodic boundary conditions are set along x-

and y-directions. Such an approach is followed in all the simulations presented in this manuscript. An excellent agreement was observed between our simulations and the results in Ref. 13 (see supplementary material). In our simulations, 2DEGs were modeled assuming an effective thickness. The frequency dependent response of the 2DEGs was described by the following Drude conductivity and permittivity

$$\sigma = \sigma_{DC}/(1+\omega^2\tau^2); \quad \epsilon = \epsilon_r - (\sigma_{DC}\tau/\epsilon_0)/(1+\omega^2\tau^2), \tag{2}$$

where τ is the electron momentum relaxation time, σ_{DC} is the 2DEG DC conductance (S/m), and ϵ_r is the low-frequency relative permittivity of the material in which the 2DEG is formed.

As discussed in Ref. 13, the quality of the plasmonic resonances increases as temperature is decreased. The reason behind the small resonance strength typically observed at room-temperature is due to a large electron-plasma-wave damping when $\omega\tau \ll 1$. In order to counteract this damping, addition of resonant-tunneling, as a gain medium, was proposed by Ryzhii and Shur in the context of terahertz detectors and oscillators.[6,7] The possibility of attaining stable terahertz power gain in these structures was later studied by Sensale-Rodriguez *et al.*[4] using a transmission line model and assuming coupling in and out of the device via antennas external to the RTD-gated HEMT. In this case, the condition that must be satisfied for maximum power gain can be expressed as[4]

$$\mathrm{NDC} = |c_{\mathrm{barrier}}/\tau|, \tag{3}$$

where NDC and c_{barrier} are the gate-to-channel negative differential conductance and the total barrier capacitance, per unit area, respectively. The unit cell sketch depicted in Fig. 1(a), which corresponds to the RTD-gated HEMT epitaxial structure discussed in Refs. 4 and 5, will be herein analyzed. However, *in this work, normally incident terahertz radiation will be coupled into electron-plasma waves in the active region of the device via the grating-gate itself as depicted in Fig. 1(b) rather than by an external antenna structure* (see Fig. 1(c)).

As discussed in Ref. 5, the plasma wave vector, k, with the addition of the gate-to-channel negative differential conductance follows the following frequency dispersion:

$$k = s^{-1}\sqrt{\omega^2 + i\omega(\tau^{-1}+\alpha^{-1}) - (\tau\alpha)^{-1}}, \tag{4}$$

where $s = (e^2 n_s)/(m^*\epsilon_r\epsilon_0)$ and $\alpha = -|c_{barrier}/NDC|$. From (4), by considering the real part of the wave vector, $Re(k)$, and by the selection rule for the first plasmon resonance, the resonance frequency reads

$$\omega_0' = 2\omega_0\sqrt{\omega_0^2 + (\tau\alpha)^{-1}} \Big/ \sqrt{4\omega_0^2 + (\tau^{-1}+\alpha^{-1})^2}, \tag{5}$$

where $\omega_0 = s\pi/2L$ is the resonance frequency in the limit when $\omega\tau \gg 1$ as defined for a structure without gate-to-channel negative differential conductance (i.e., $\alpha \to \infty$, $\tau \to \infty$). As observed from (5), in the vicinity of the point where the condition for maximum gain is satisfied, i.e., (3),

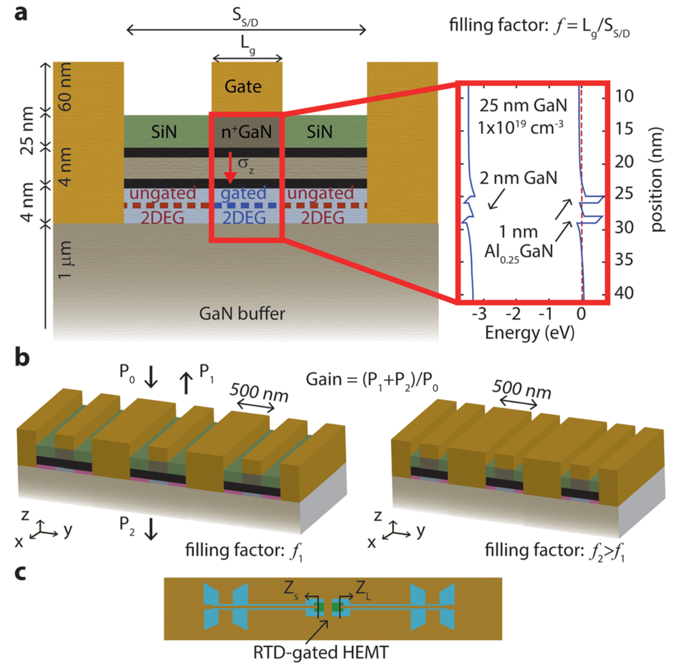

FIG. 1. (a) Unit cell epitaxial structure of the analyzed RTD-gated HEMTs. All layers are modeled employing Drude models for their frequency dependent electrical conductivities, the two layers depicted in black color correspond to AlGaN barriers. (b) Sketch of grating-gate devices with two different filling factors. Filling factor, f, is defined as the ratio between the gate length (L_g) and the source-to-drain separation ($S_{S/D}$) as defined in (a). (c) Sketch of an antenna coupled device configuration (top view).

adding negative differential conductance into the structure leads to a red-shift on the frequency of resonance. In general, it follows from (4) that:

$$\omega_0' \propto \sqrt{\xi - |NDC|}, \tag{6}$$

where the parameter ξ is independent of the negative differential conductance level in the structure but dependent on the structure geometry, 2DEG conductivity level, and materials parameters.

Since electron-tunneling occurs along the z-direction, the dynamic-conductivity of the AlGaN/GaN/AlGaN tunneling region is modeled through an anisotropic-material tensor (i.e., $\sigma_x = \sigma_y = 0$, $\sigma_z < 0$). *The z-component of its conductivity (σ_z) is varied in our simulations* in a proper interval around $\sigma_z \approx -\frac{\varepsilon_{\mathrm{barrier}}}{\tau} \approx -600$ S/m, in agreement with Eq. (3). No frequency dispersion is assumed for this region owing to the fact that the estimated dwell-time for the RTD structure, which contains thin AlGaN barriers (1 nm) of low Al composition (25%) (as depicted in Fig. 1(a)), is on the order of 10 fs, and thus $\omega\tau_{\mathrm{dwell}} \ll 1$. Also, due to the low Al composition of the barriers, an effective relative permittivity of 9.5 is assumed for the AlGaN/GaN/AlGaN tunneling region. All other material layers are modeled following Drude models and proper relative permittivity values, i.e., 9.5 for GaN and 7 for SiN; DC conductivities of 2.4×10^4 and 230 S/m, and τ of 75 and 150 fs are assumed for the n + GaN region above the tunneling region and for the GaN buffer layer below the HEMT channel, respectively. In all our numerical simulations, we considered devices with a gate-length of 100 nm. The thicknesses of various material layers, together with a zero-bias band diagram along the z-direction (below the

gate), are depicted in Fig. 1(a). The gated 2DEG, as well as the ungated 2DEG, was modeled as 4 nm thick conductive layers following a Drude-dispersion where τ was set to 130 fs, following the discussion in Ref. 19; and the source/drain electrode contact length was fixed to 500 nm. The filling-factor is defined as the ratio between the gate length (L_g) and the source-to-drain separation ($S_{S/D}$), as pictured in Fig. 1(a). *The gated/ungated 2DEG conductivity as well as the filling-factor was also varied in our simulations*. In the following discussion, *power gain* will be defined as the ratio (in dB) between: (i) the sum of the powers of the reflected (P_1) and transmitted waves (P_2) through the structure and (ii) the power of the incoming terahertz excitation (P_0), i.e., $(P_1 + P_2)/P_0$ as shown in Fig. 1(b).

At this end, we performed numerical simulations using a layer-by-layer model in HFSS employing a frequency resolution of 5 GHz. In our *first set of simulations*, we varied (i) the negative differential conductance σ_z and (ii) the ungated-region sheet conductivity, while keeping fixed (a) the filling-factor ($f = 0.3$) and (b) the gated-region sheet conductivity ($\sigma_{DC,gated} = 2$ mS). Our analysis shows that the ungated 2DEG region heavily affects the response of the structure. Figure 2(a) depicts the extracted maximum gain (i.e., maximum in the gain spectra) for two different values of ungated sheet conductivity, namely, 0 and 3 mS, as a function of σ_z. It is observed that *with zero ungated conductivity no gain can take place, regardless of the negative differential conductance level*. In order to further understand the effect of the ungated conductivity on the device response, in Fig. 2(b) we show the Poynting vector distribution under the conditions for maximum gain in Fig. 2(a) (i.e., negative differential conductance level and frequency set to the values where maximum gain is observed). The Poynting vector distribution shows that *the reason behind no gain being observed in structures with zero ungated conductivity, i.e., no 2DEG in the ungated region, is because the incoming terahertz radiation needs to be coupled into the gated-region (gain medium) via the ungated region*. Figure 2(c) shows the gain spectra for a configuration with $\sigma_{DC,ungated} = 3$ mS when varying σ_z. It is observed, in agreement with the discussion in Ref. 4, *that there exists a certain value of σ_z capable of maximizing the attainable gain*; however, this value is around 4× larger than what is predicted by Eq. (3). The reason behind this observation might be due to additional loss induced by the finite doping in the RTD access region and in the buffer layer as well as by the frequency dispersion assumed for such layers, which are effects not accounted for in previous transmission line models.[4] Although in the GaN materials system experimental demonstrations to date have not shown strong resonant characteristics, it is worth mentioning that RTDs in InAlGaAs have been demonstrated capable of providing the required negative differential conductance levels.[20] Moreover, we also observe that the frequency of resonance depends on the negative differential conductance levels. This effect is captured in Fig. 2(d), where the effect of negative differential conductance on the frequency of resonance is analyzed for a device configuration with $\sigma_{DC,ungated} = 3$ mS. It is observed that *as σ_z is increased, the resonance frequency red-shifts*, which is consistent with the trend predicted by Eq. (6).

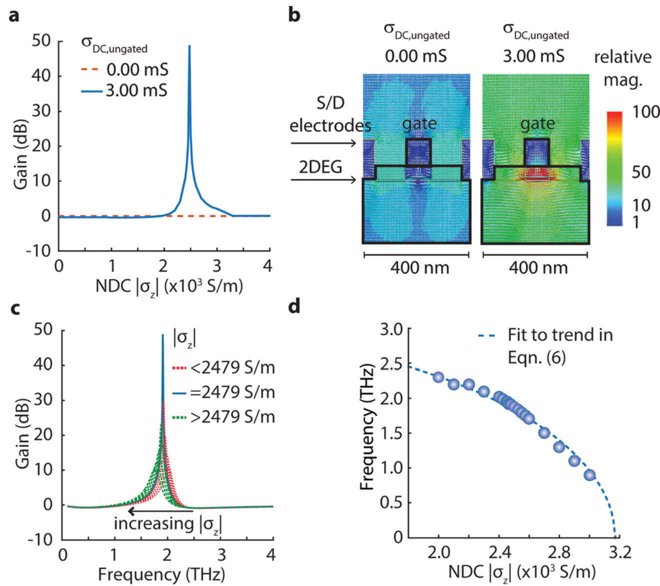

FIG. 2. (a) Extracted maximum gain (from the calculated gain spectra) for a configuration with 2 mS gated DC sheet conductivity, and 0 (dashed) and 3 mS (continuous) ungated DC sheet conductivity, as a function of the negative differential conductance $|\sigma_z|$. (b) Poynting vector profile (relative magnitude) at 2 THz for 0 mS (left) and 3 mS (right) ungated DC sheet conductivity, in both cases the gated DC sheet conductivity is fixed to 2 mS; coupling of electromagnetic waves into the active region of the device is observed only when having a finite ungated conductivity. (c) Corresponding gain spectra used to extract the maximum gain shown in (a). The RTD negative differential conductance is swept and the DC sheet conductivities of the gated and ungated regions are fixed to 2 mS and 3 mS, respectively (d) Extracted resonance frequency as a function of the negative differential conductance $|\sigma_z|$ for a device configuration with 2 mS gated sheet conductivity and 3 mS ungated DC sheet conductivity. In all cases, the gate length and filling factor are set to 100 nm and 0.3, respectively.

In our *second set of simulations*, we analyzed the effect of gated and ungated conductivity on the resonance frequency. For this purpose, we varied (i) the gated-region sheet conductivity and (ii) the ungated-region sheet conductivity, while keeping fixed (a) the filling factor ($f = 0.3$) and (b) the negative differential conductance ($\sigma_z = 2479$ S/m). $\sigma_z = 2479$ S/m is chosen since this was the value leading to the maximum gain observed in the design space exploration discussed in Fig. 2. Figure 3(a) analyzes the effect of the conductivity of the gated-region on the location of the plasmonic resonance frequency. Simulations were performed by varying $\sigma_{DC,gated}$ while keeping the ungated-region sheet conductivity fixed to $\sigma_{DC,ungated} = 3$ mS. In accordance with Eqs. (1) and (4), it is observed that *as the gated conductivity is increased the frequency of resonance blue-shifts*. In contraposition, the effect of the ungated-region conductivity on the frequency of resonance is much weaker. Figure 3(b) shows the gain spectra for different values of $\sigma_{DC,ungated}$ and a fixed gated-region sheet conductivity of $\sigma_{DC,gated} = 2$ mS. Although a frequency blue-shift is observed as the ungated conductivity increases, the noticed dependence is much weaker than that observed when altering the gated-region conductivity (see Fig. 3(a)) or the negative differential conductance (see Fig. 2(d)). Therefore, it is concluded that *the main effect of the ungated region is on enabling the radiation coupling*.

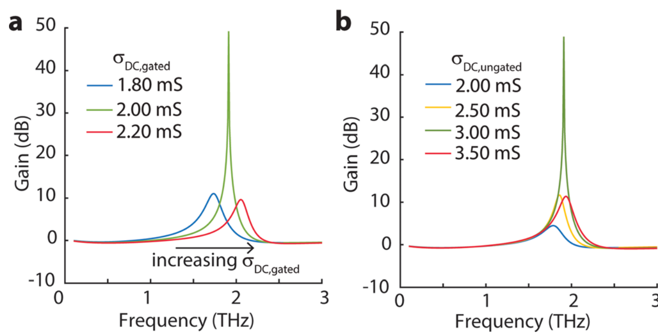

FIG. 3. (a) Gain spectra for device configurations with varying gated conductivity. The ungated region DC sheet conductivity, negative differential conductance, and filling factor are set to 3 mS, 2479 S/m, and 0.3, respectively. (b) Gain spectra for device configurations with varying ungated conductivity. The gated region DC sheet conductivity, negative differential conductance, and filling factor are set to 2 mS, 2479 S/m, and 0.3, respectively.

In our *third set of simulations*, *we show how our analysis can also provide information about potential instabilities in the device*. Figure 4 depicts the gain spectra for two device configurations with 0.5 and 2 mS ungated-region sheet conductivity, respectively. In both cases, the gated-region sheet conductivity was set to $\sigma_{DC,gated} = 0.5$ mS, the filling-factor was set to $f = 0.3$, and σ_z was chosen to that maximizing gain. Although gain is observed in both situations, when carefully analyzing the low-frequency end of the spectra (inset in Fig. 4), it is observed that when $\sigma_{DC,ungated} = 2$ mS the power gain can be potentially unstable, i.e., gain is observed even at zero frequency, which is signature of potential DC device instability. The reason behind why, although having the same gated-region conductivity, gain peaks at different frequencies in the configurations analyzed in Fig. 4 are due to the negative differential conductance levels leading to maximum gain being different in the two configurations.

Overall, our results indicate that terahertz radiation can be effectively coupled into electron plasma waves in the gated region, and power amplification can be observed at resonance. When sweeping all the design parameters, it is observed that a maximum stable power gain of ~48 dB can take place. For reference, our previous work on RTD-gated HEMTs, employing antenna fed configurations, also predicts power amplification but with a much lower gain (around 5 dB) at such frequencies.[4] In this regard, it is worth mentioning that in an antenna fed amplifier configuration, the load and generator impedances should be designed so that proper impedance matching takes place. In our previous work, these impedances were considered as frequency independent, which gives rise to amplification of higher order resonant modes (i.e., multiple peaks in the gain spectra); however, in practice, this is difficult to attain. In this work, we observe that the grating gate configuration enhances the coupling mainly for the first resonance and the coupling efficiency reduces for higher order resonances as seen experimentally, e.g., Ref. 13. Another reason behind the larger observed gain levels, besides efficient electromagnetic coupling, is that the stability conditions seem to be relaxed from those under antenna feed configurations, therefore leading to a higher stable gain than that in our previous work. Scrutinizing this difference will be the focus of future work.

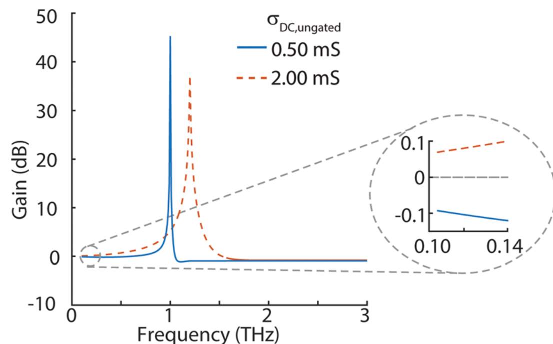

FIG. 4. Gain spectra for configurations exhibiting maximum gain with varying ungated conductivity. The pictured cases correspond to configurations leading to maximum gain when sweeping negative differential conductance. The gated DC sheet conductivity is set to 0.5 mS and the filling factor to 0.3. Two cases corresponding to ungated DC sheet conductivity of 0.5 mS (continuous) and 2 mS (dashed) are pictured. When the ungated conductivity is set to 2 mS, gain is observed even at zero frequency, which is signature of potential DC device instability.

Finally, in our *fourth set of simulations*, we analyzed the effect of the filling-factor, when varying the gated and ungated conductivities and negative differential conductance levels so to optimize gain (as per the previous discussion). Figure 5 shows the tabulated maximum gain (dB) for different combinations of gated and ungated region conductivities for different filling-factors (for a fixed gate length of $L_g = 100$ nm in accordance with previous simulations). σ_z was swept and the maximum extracted stable gain (i.e., maximum in the gain spectra) was tabulated in each of the tables depicted in Figs. 5(a)–5(c); table entries labeled in red as "0" dB represent situations where no stable designs were found, i.e., when sweeping the negative differential conductance the gain spectra always show gain at zero frequency; thus, all cases constitute potentially unstable designs in accordance

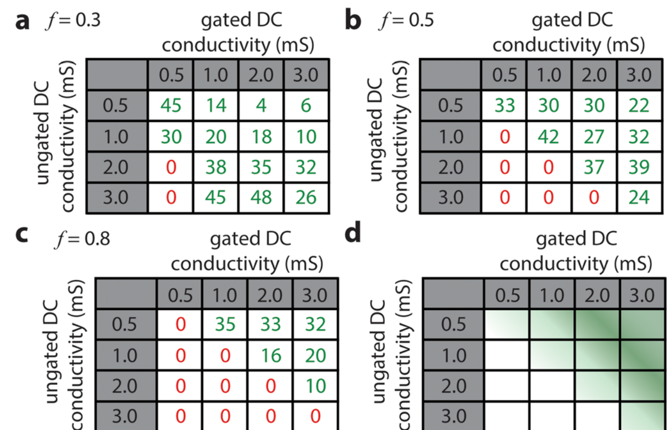

a $f = 0.3$

ungated DC conductivity (mS) \ gated DC conductivity (mS)	0.5	1.0	2.0	3.0
0.5	45	14	4	6
1.0	30	20	18	10
2.0	0	38	35	32
3.0	0	45	48	26

b $f = 0.5$

ungated DC conductivity (mS) \ gated DC conductivity (mS)	0.5	1.0	2.0	3.0
0.5	33	30	30	22
1.0	0	42	27	32
2.0	0	0	37	39
3.0	0	0	0	24

c $f = 0.8$

ungated DC conductivity (mS) \ gated DC conductivity (mS)	0.5	1.0	2.0	3.0
0.5	0	35	33	32
1.0	0	0	16	20
2.0	0	0	0	10
3.0	0	0	0	0

FIG. 5. (a)–(c) Simulated maximum power gain for different filling factors (f): 0.3, 0.5, and 0.8, respectively, and fixed gated/ungated DC sheet conductivity levels as indicated by the table axes. For these gated/ungated conductivity combinations, the negative differential conductance (σ_z) was swept; the gain levels listed in the table correspond to optimal configurations with σ_z leading to maximum gain. Table entries labeled in red as "0" dB represent situations where no stable designs were found, i.e., when sweeping σ_z the gain spectra always show gain at zero frequency; thus, all configurations constitute potentially unstable designs. (d) Observed trends for designs exhibiting maximum gain. Configurations attaining maximum gain shift from the non-colored region to the green-colored region of the table when f is increased.

with the discussion in Fig. 4. In general, it is observed that *as the filling-factor is increased, an optimal design for maximum stable gain requires higher gated-region conductivity relative to the conductivity of the ungated-region*, i.e., as depicted in Fig. 5(d), the designs attaining maximum gain shift from the non-colored region to the green-colored region of the table as f is increased. *In accordance with previous discussion, in all cases it was observed that a finite ungated conductivity is required to provide terahertz power amplification.*

In conclusion, this paper predicts terahertz power amplification in RTD-gated HEMTs with a grating-gate coupling topology. Terahertz radiation in these devices is coupled into 2DEG channel plasmons via the grating-gate itself, rather than by an antenna structure as in previous works. The potential of achieving power amplification with gain exceeding 40 dB at ∼2 THz is predicted. The electrical conductivities of the gated and ungated regions, the negative differential conductance level achievable from the RTD, and the filling-factor are identified as key parameters affecting the attainable power gain levels as well as the stability in this device.

See supplementary material for our simulation results of the structure analyzed in Ref. 13.

This work was supported by the Office of Naval Research, N00014-11-1-0721, Devices and Architectures for THz Electronics MURI, Paul Maki program manager. This work was also supported by the NSF MRSEC program at the University of Utah under Grant No. # DMR 1121252 and by NSF ECCS #1407959. The support and resources from the Center for High Performance Computing at the University of Utah are gratefully acknowledged.

[1]M. Tonouchi, Nat. Photonics **1**, 97–105 (2007).
[2]T. Otsuji and M. Shur, IEEE Microwave Mag. **15**, 43–50 (2014).
[3]P. H. Siegel, IEEE Trans. Microwave Theory Tech. **50**, 910–928 (2002).
[4]B. Sensale-Rodriguez, L. Liu, P. Fay, D. Jena, and H. G. Xing, IEEE Trans. Terahertz Sci. Technol. **3**, 200–206 (2013).
[5]B. Sensale-Rodriguez, P. Fay, L. Liu, D. Jena, and H. G. Xing, ECS Trans. **49**, 93–102 (2012).
[6]V. Ryzhii and M. Shur, Jpn. J. Appl. Phys., Part 1 **40**, 546 (2001).
[7]V. Ryzhii, I. Khmyrova, and M. Shur, J. Appl. Phys. **88**(5), 2868–2871 (2000).
[8]V. Popov, J. Infrared, Millimeter, Terahertz Waves **32**(10), 1178–1191 (2011).
[9]M. Dyakonov and M. S. Shur, IEEE Trans. Electron Devices **43**(10), 1640–1645 (1996).
[10]M. Dyakonov and M. S. Shur, Phys. Rev. Lett. **71**(15), 2465–2468 (1993).
[11]T. Otsuji, M. Hanabe, T. Nishimura, and E. Sano, Opt. Express **14**(11), 4815–4825 (2006).
[12]T. Otsuji, Y. Meziani, M. Hanabe, T. Ishibashi, T. Uno, and E. Sano, Appl. Phys. Lett. **89**(26), 263502 (2006).
[13]A. V. Muravjov, D. B. Veksler, V. V. Popov, O. V. Polischuk, N. Pala, X. Hu, R. Gaska, H. Saxena, R. E. Peale, and M. S. Shur, Appl. Phys. Lett. **96**(4), 042105 (2010).
[14]T. Otsuji, Y. M. Meziani, T. Nishimura, T. Suemitsu, W. Knap, E. Sano, T. Asano, and V. V. Popov, J. Phys.: Condens. Matter **20**(38), 384206 (2008).
[15]S. Allen, D. Tsui, and R. Logan, Phys. Rev. Lett. **38**(17), 980–983 (1977).
[16]L. Ju, B. Geng, J. Horng, C. Girit, M. Martin, Z. Hao, and F. Wang, Nat. Nanotechnol. **6**(10), 630–634 (2011).
[17]A. Eguiluz, T. Lee, J. Quinn, and K. Chiu, Phys. Rev. B **11**, 4989 (1975).
[18]S. Das Sarma and A. Madhukar, Phys. Rev. B **23**, 805 (1981).
[19]P. Burke, I. Spielman, J. Eisenstein, L. Pfeiffer, and K. West, Appl. Phys. Lett. **76**(6), 745 (2000).
[20]M. Feiginov, H. Kanaya, S. Suzuki, and M. Asada, Appl. Phys. Lett. **104**(24), 243509 (2014).